THE JOURNAL OF PHYSICAL CHEMISTRY A

Subscriber access provided by LAWRENCE BERKELEY NATL LAB

Article

Enhanced Light Absorption and Scattering by Carbon Soot Aerosol Internally Mixed with Sulfuric Acid

Alexei F. Khalizov, Huaxin Xue, Lin Wang, Jun Zheng, and Renyi Zhang

J. Phys. Chem. A, **2009**, 113 (6), 1066-1074• DOI: 10.1021/jp807531n • Publication Date (Web): 15 January 2009

Downloaded from http://pubs.acs.org on February 24, 2009

More About This Article

Additional resources and features associated with this article are available within the HTML version:

- Supporting Information
- Access to high resolution figures
- Links to articles and content related to this article
- Copyright permission to reproduce figures and/or text from this article

View the Full Text HTML

ACS Publications
High quality. High impact.

The Journal of Physical Chemistry A is published by the American Chemical Society. 1155 Sixteenth Street N.W., Washington, DC 20036

Enhanced Light Absorption and Scattering by Carbon Soot Aerosol Internally Mixed with Sulfuric Acid

Alexei F. Khalizov, Huaxin Xue, Lin Wang, Jun Zheng, and Renyi Zhang*

Department of Atmospheric Sciences and Department of Chemistry, Texas A&M University, College Station, Texas 77843

Received: August 22, 2008; Revised Manuscript Received: November 20, 2008

Light absorption by carbon soot increases when the particles are internally mixed with nonabsorbing materials, leading to increased radiative forcing, but the magnitude of this enhancement is a subject of great uncertainty. We have performed laboratory experiments of the optical properties of fresh and internally mixed carbon soot aerosols with a known particle size, morphology, and the mixing state. Flame-generated soot aerosol is size-selected with a double-differential mobility analyzer (DMA) setup to eliminate multiply charged particle modes and then exposed to gaseous sulfuric acid (10^9-10^{10} molecule cm^{-3}) and water vapor (5−80% relative humidity, RH). Light extinction and scattering by fresh and internally mixed soot aerosol are measured at 532 nm wavelength using a cavity ring-down spectrometer and an integrating nephelometer, respectively, and the absorption is derived as the difference between extinction and scattering. The optical properties of fresh soot are independent of RH, whereas soot internally mixed with sulfuric acid exhibits significant enhancement in light absorption and scattering, increasing with the mass fraction of sulfuric acid coating and relative humidity. For soot particles with an initial mobility diameter of 320 nm and a 40% H_2SO_4 mass coating fraction, absorption and scattering are increased by 1.4- and 13-fold at 80% RH, respectively. Also, the single scattering albedo of soot aerosol increases from 0.1 to 0.5 after coating and humidification. Additional measurements with soot particles that are first coated with sulfuric acid and then heated to remove the coating show that both scattering and absorption are enhanced by irreversible restructuring of soot aggregates to more compact globules. Depending on the initial size and density of soot aggregates, restructuring acts to increase or decrease the absorption cross-section, but the combination of restructuring and encapsulation always results in an increased absorption for internally mixed soot. Mass absorption cross-sections (MAC) for fresh soot aggregates are size dependent, increasing from 6.7 ± 0.7 m^2 g^{-1} for 155 nm particles to 8.7 ± 0.1 m^2 g^{-1} for 320 nm particles. After exposure of soot to sulfuric acid, MAC is as high as 12.6 m^2 g^{-1} for 320 nm particles at 80% RH. Our results imply that optical properties of soot are significantly altered within its atmospheric lifetime, leading to greater impact on visibility, local air quality, and radiative climate forcing.

1. Introduction

Atmospheric aerosols perturb the radiation balance of the Earth and affect the regional and global climate, directly through scattering and absorption of solar radiation or indirectly by acting as cloud condensation nuclei (CCN). The changes in radiative fluxes induced by aerosols, referred to as the aerosol direct radiative forcing, is an important component of climate forcing.[1] Aerosol particles not only reflect solar light back to space, cooling the Earth's surface, but also absorb the solar energy, heating the atmosphere. Absorption of visible radiation by airborne particles is primarily due to soot and mineral dust. Hence, the optical properties of soot-containing aerosols directly impact the atmospheric visibility as well as local and global climate. A recent study reveals that in the areas identified as aerosol hotspots, which include 13 megacities, atmospheric solar heating caused by soot-containing aerosols is roughly comparable with the heating due to greenhouse gases.[2] In addition, light absorption by soot-containing aerosols reduces photolysis at the surface level, impacting photochemistry,[3] and inhibits cloud formation and precipitation.[4]

The variation in the reported mass absorption cross-sections (MAC) of soot represents one of the major factors leading to large uncertainties in the evaluation of the atmospheric optical effects.[5] The discrepancies in MAC are likely caused by variations in soot morphology and complex refractive index and by inaccurate or inconsistent material density.[6,7] Moreover, freshly emitted soot is subjected to several aging processes in the atmosphere that may affect its optical properties, particularly in polluted regions. These processes include adsorption and condensation of gaseous species on the soot surface,[8,9] coagulation of soot with other pre-existing aerosol constituents,[10] and oxidation of soot by various atmospheric species.[11] Internally mixed soot aerosol is also produced from burning sulfur-containing fuels.[12]

Field measurements indicate that during transport from the sources, fresh soot becomes internally mixed with sulfates and organics, leading to enhancement in light absorption by about 30%.[13,14] These observations confirm the results of modeling calculations that an internal mixture of soot with other aerosol components is significantly more absorptive than the external mixture.[6,15] The fractal-like structure of soot aggregates undergoes a significant restructuring during internal mixing, resulting in compact cores. A range of theoretical approaches have been used to treat the optical properties of carbon soot aggregates

* Corresponding author. Tel: 979-845-7656, fax 979-862-4466, e-mail zhang@ariel.met.tamu.edu.

10.1021/jp807531n CCC: $40.75 © 2009 American Chemical Society
Published on Web 01/15/2009

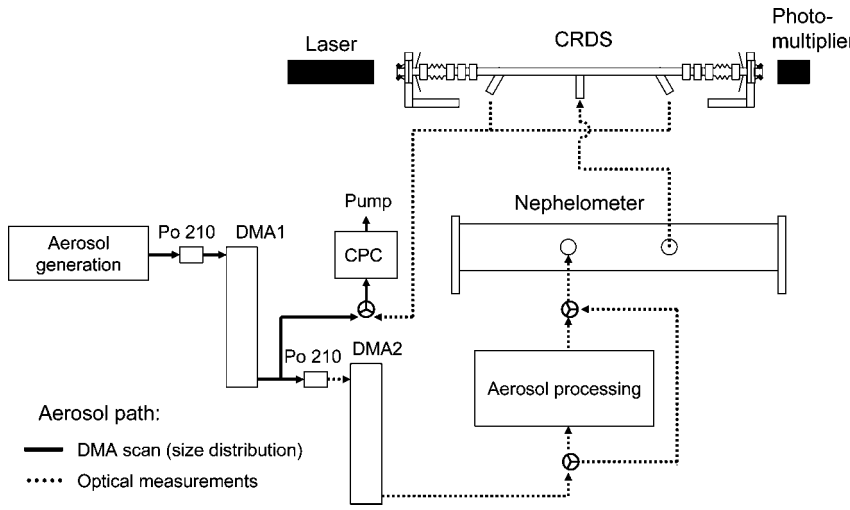

Figure 1. Schematic diagram of the experimental setup for measurements of light extinction and scattering by soot particles.

and their mixtures with dielectric coatings.[6,16,17] However, the complex variation in morphology of soot agglomerates that occurs during atmospheric processing and undoubtedly contributes to changes in the optical properties of aged soot is difficult to be accounted for in theoretical calculations. Commonly used representation of aged soot particles as an ideal mixture of the absorbing and transparent materials (effective medium theories) is rather unphysical and can lead to unrealistically high absorption. Radiative transfer models assuming externally mixed configuration for atmospheric soot overestimate the aerosol cooling effect, whereas models using well-mixed assumption underestimate the cooling effect.[16]

Despite the ample field and modeling studies on the variable optical properties of soot particles during atmospheric aging, there exist only a few laboratory measurements where the effect of internal mixing on soot optical properties has been investigated.[18−20] These previous studies focused on the change in morphology and optical properties of fresh soot mixed with organic materials represented by ozonolysis products of α-pinene,[18] glutaric acid,[19] and carnauba wax.[20] Furthermore, despite the abundance of observational evidence of soot aerosols internally mixed with sulfuric acid whose spectroscopic properties have been extensively studied experimentally,[21,22] no laboratory study is currently available on the optical properties of soot particles exposed to gaseous sulfuric acid in a controlled manner.

In this paper, we present the laboratory measurements of optical properties of fresh soot and soot exposed to gaseous sulfuric acid and water vapor to mimic atmospheric processing. The morphology, mixing state, and hygroscopic properties of these particles, studied in great detail, are reported elsewhere.[23,24] Ongoing work in our group also includes investigation of effects of soot aging due to exposure to organic compounds, which are produced when volatile organic compounds are oxidized in the atmosphere.[25]

2. Experimental Section

A diagram of the experimental setup used to measure the optical properties of soot-containing aerosols is shown in Figure 1. The main components include an aerosol generation system, two differential mobility analyzers (DMA1 and DMA2) to produce mobility-classified, singly charged aerosol particles, an aerosol coating and humidification system to simulate atmospheric processing, an integrating nephelometer and a cavity ring-down spectrometer (CRDS) to measure the scattering and extinction of light by aerosol, and a condensation particle counter (CPC) to measure the aerosol particle number density.

2.1. Aerosol Generation and Processing. The aerosol generation and processing procedures are reported in more detail by Khalizov et al.,[23] and only a brief description is provided here. Carbon soot aerosol is generated by incomplete combustion of propane in a laminar diffusion burner[26] and sampled using a pinhole diluter.[27] The diffusion flame produces stable aerosol concentration, and the particles contain essentially no organic carbon.[28] A flame equivalence ratio of about 0.5 is used throughout this study (the actual fuel to oxygen ratio divided by the fuel to oxygen ratio under stoichiometric conditions) to maintain a constant size distribution with a geometric mean diameter of 130 nm and geometric standard deviation of 1.8. Polystyrene latex spheres (PSL, Duke Scientific Inc., USA), ammonium sulfate (ACS grade, Mallinckrodt Baker, Inc.), and sodium chloride (ACS grade, EMD Chemicals, Inc.) aerosols are generated from corresponding solutions in deionized water (17 MΩ) using a constant output atomizer (3076, TSI Inc.). Particles from both sources, the flame and the atomizer, are diluted with a dry nitrogen flow and passed through a silica gel diffusion drier, a Nafion multitube drier (PD-070-18T-12SS, Perma Pure Inc.), and a bipolar charger (^{210}Po, 400 μCi) prior to entering DMA1. Particles from DMA1 are recharged in the second diffusion charger and size-selected by DMA2. The sheath and sample flow rates in both DMAs are maintained at 6.5 and 1.0 L min^{-1}, respectively.

Singly charged, mobility-classified aerosol particles produced by the DMA−DMA setup are admitted to an aerosol processing unit, which consists of a H_2SO_4 condensation chamber, a Nafion humidifier, a Nafion drier, and a heater. The flow rate through the aerosol processing unit is equal to the DMA sample flow rate, 1.0 L min^{-1}. The condensation chamber [8,23] is used to expose aerosol particles to sulfuric acid vapor. It consists of a 50 cm long, 3 cm inner diameter horizontal Pyrex container filled to about half with aqueous sulfuric acid solution. The residence time of aerosol in the chamber is about 12 s, and the temperature is maintained at 26 ± 1 °C. The concentration of H_2SO_4 vapor in the coating chamber is measured using ion drift−chemical ionization mass spectrometry (ID-CIMS),[29−31] in the range of 1.4×10^{10} (high) and 2.5×10^{9} (low) molecule cm^{-3}. To stabilize sulfuric acid against evaporation on the coated particles, the aerosol flow is humidified to RH 5% downstream

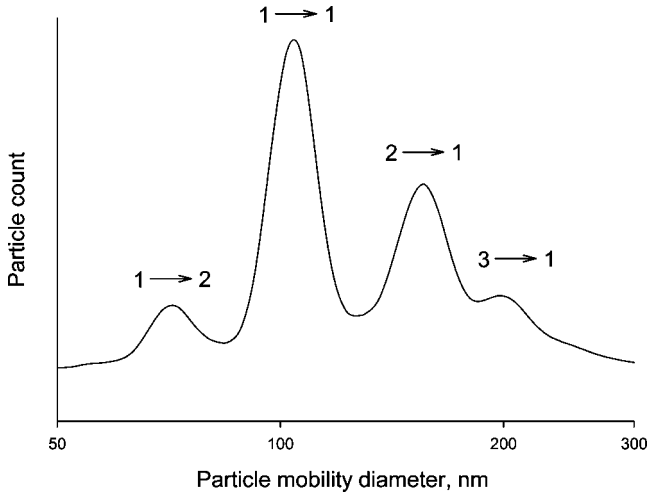

Figure 2. A TDMA scan showing the presence of multiply charged particles in the mobility-classified fresh (uncoated) soot aerosol produced by DMA1. The DMA1 voltage is set to transmit particles with mobility diameter 100 nm while the DMA2 voltage is scanned. An additional Po-210 diffusion charger is placed in front of DMA2. Major recharging processes are indicated above the corresponding modes, e.g. "2→1" stands for doubly charged particles which become singly charged after passing through the second diffusion charger. The location for the "1→1" peak at 105 nm is due to a minor mismatch between DMA1 and DMA2 flows and voltages.

the condensation chamber. The heater is operated at 200 °C to remove condensed volatile material.[32]

2.2. Multiply Charged Particles in Soot Aerosol. A dual DMA system is employed in this study to generate monodisperse aerosol for the optical measurements because a single DMA, in addition to selected particles, transmits larger multiply charged particles. In a DMA, the particles are sized according to their electrical mobility, Z_p, which is related to the particle mobility diameter, D_p, particle charge, q, and Cunningham slip correction, $C(D_p)$

$$Z_p \propto \frac{q \times C(D_p)}{D_p} \quad (1)$$

When particles with mobility diameter D_p and charge $q = 1$ are selected, larger particles with charges $q = 2, 3, \ldots n$ that satisfy the condition given by eq 1 are also transmitted. The number of observed modes (n) and their relative intensities depend on the shape of the polydisperse distribution and selected D_p. For instance, in the case of polydisperse ammonium sulfate aerosol, doubly and triply charged particles with mobility diameters of $\sim 1.5 \times D_p$ and $\sim 1.7 \times D_p$ pass through the DMA along with singly charged particles. Multiply charged particles, because of their larger effective size, scatter and absorb light more efficiently than singly charged particles of the same electrical mobility. Since light absorption and scattering vary nonlinearly with the particle size, even a small fraction of these larger particles in aerosol can lead to significant overestimation of the measured optical cross-sections.

The presence of multiply charged particles in the mobility-classified aerosol can be revealed by using an additional charger and a second DMA in series with DMA1. As shown in Figure 2, four distinct modes are distinguished in the propane soot aerosol when DMA1 voltage is set to transmit particles with $D_p = 100$ nm while DMA2 voltage is scanned. The most intense mode at about 100 nm corresponds to singly charged particles. A mode at ~70 nm is produced when some of these 100 nm particles become doubly charged after passing through the second diffusion charger. The modes at 155 and 200 nm correspond to the particles that emerge from DMA1 with two and three charges, respectively, but become singly charged after passing through the second diffusion charger. We find that the mode at 155 nm (or about $1.5 \times D_p$ for any arbitrary D_p) produces the best agreement between experimentally measured and calculated (Mie) scattering coefficient for crystalline ammonium sulfate aerosol. This mode contains the smallest fraction of multiply charged particles and hence is used to study the effect of processing on the optical properties of soot. Aerosol from DMA1, which is adjusted to transmit particles with mobility diameter D_p, passes through the diffusion charger and then through DMA2, which transmits only particles with mobility diameter of about $1.5 \times D_p$. Table 1 presents the mobility diameters for DMA2 determined experimentally from TDMA scans of soot aerosol at three different values of D_p.

TABLE 1: Mobility Diameter Settings for DMA1 and DMA2 Used To Generate Monodisperse Aerosol and Corresponding Effective Densities of Fresh Soot Particles

D_p, nm		
DMA1	DMA2	Effective density [a], g cm^{-3}
100	155	0.26
155	245	0.17
195	320	0.12

[a] Interpolated from effective densities of fresh soot measured under identical experimental conditions.[24]

Addition of the second DMA significantly narrows the size distributions but does not completely eliminate the contribution from multiply charged particle modes. Experimentally measured scattering cross-sections for crystalline ammonium sulfate aerosol classified using the dual DMA system are 17−47% higher than the values calculated with Mie theory (larger error for smaller particles). In a similar test with PSL spheres, the measured scattering cross-sections are 2−12% higher than the calculated values (larger error for smaller particles). Also, we find little difference between the measurements where PSL aerosol is mobility-classified using a single DMA or the dual DMA system because commercial polystyrene latex spheres have very narrow particle size distribution and the probability of having multiply charged particles satisfying eq 1 is negligible. The remaining discrepancy, decreasing with increasing particle size, can be caused by the residue of surfactant left on the PSL surface after evaporation of the aerosol droplet. Finally, we estimate that the bias in the optical measurements due to remaining multiply charged particles is significantly smaller for soot aerosol than for ammonium sulfate. The effective density of soot particles decreases with mobility size (Table 1) and so does the contribution to scattering and absorption cross-sections from multiply charged particles.

2.3. Measurements of Aerosol Optical Properties. Optical properties of aerosol particles at 532 nm wavelength are measured using a combination of a CRDS and a nephelometer interfaced to the DMA−DMA system (Figure 1).

Aerosol extinction is measured by the CRDS.[33] A light pulse (532 nm, pulse energy 100 μJ, pulse duration 11 ns) produced by a Q-switched pulsed laser (CrystaLaser QG-532-500) is injected into a cavity formed by two high-reflectivity dielectric mirrors (540 nm center wavelength, 99.9985% reflectivity, 6 m radius of curvature, 0.8 in. diameter, Los Gatos Research, Inc.) and a stainless steel cell equipped with aerosol inlet and outlet. The distance between mirrors and the sample length are 72 and 43 cm, respectively. To prevent the mirrors from contamination by aerosol, the mirror region is purged with a small flow of dry

nitrogen (2−4% of the aerosol sample flow). Light exiting the cavity is detected with a Hamamatsu H6780-02 photomultiplier. The output of the photomultiplier is digitized by a 100 MHz, 16-bit resolution CompuScope 12100 card (GaGe Applied Technologies, LLC) operated by LabVIEW software. Typically, 300 ring-down traces are averaged at 20 Hz repetition rate, and the decay time is calculated by nonlinear fitting of the averaged decay data. The light extinction coefficient, b_{ext}, is calculated using the decay times of the cavity with and without the aerosol sample at the same relative humidity according to eq 2

$$b_{ext} = \frac{R_L}{c}\left(\frac{1}{\tau} - \frac{1}{\tau_0}\right) \quad (2)$$

where R_L is the ratio of optical cavity length to sample length, c is the speed of light, τ is the ring-down time with sample present, and τ_0 is the ring-down time in the absence of sample.

Aerosol total scattering is measured by a commercial three-color integrating nephelometer (TSI 3563). The nephelometer is periodically calibrated according to the manufacturer's manual using carbon dioxide and nitrogen as high- and low-span gases. The systematic errors due to the nephelometer nonidealities (scattering angular truncation and deviation of the illumination intensity from cosine-weighted distribution) are corrected according to previously established procedures.[34] The scattering coefficient at 532 nm is calculated from a power law fit to the scattering coefficients at the three nephelometer wavelengths (450, 550, and 700 nm).

During optical measurements, an aerosol flow from the DMA−DMA system is directed through or bypasses the sulfuric acid condensation chamber, humidifier, and heater before being introduced consecutively through the nephelometer, CRDS, and CPC (TSI 3760A). The absorption coefficient is calculated from the difference between the extinction and scattering coefficients. The particle number density measured by CPC is used together with extinction, scattering, and absorption coefficients to calculate the corresponding cross-sections

$$C = \frac{b}{N} \quad (3)$$

where C is the cross-section and N is the particle number density. Typically, aerosol number density was adjusted between 500 and 3000 particles cm^{-3} (higher concentration for smaller particles) to maintain the extinction and scattering coefficients in the range 1−50 Mm^{-1}. Mass absorption cross-sections of soot, σ_{abs}, are calculated using effective densities of soot particles, ρ, measured by DMA−APM (aerosol particle mass) analyzer under conditions identical to those used in our previous experiments,[24]

$$\sigma_{abs} = \frac{6C_{abs}}{\rho \times \pi \times D_p^3} \quad (4)$$

For the mobility size range studied, particle losses inside the CRDS cell are negligible. To account for particle losses caused by diffusion and electrostatic precipitation in the nephelometer, size-dependent transmission coefficients are applied to particle concentrations measured by CPC. The transmission coefficients are in the range 0.7−0.9 for 155−360 nm particles (higher transmission for larger particles). Validity of this approach is confirmed by a close agreement between extinction and scattering coefficients for nonabsorbing PSL spheres measured with nephelometer and CRDS.

Light extinction and scattering by hygroscopic aerosol is a strong function of relative humidity. To eliminate the effect of dry mirror cleansing flow, the aerosol flow in the CRDS cell is directed from the center toward the mirrors and the cell is placed after the nephelometer (Figure 1). Maintaining a constant temperature throughout the entire system is also crucial for accurate measurements of aerosol optical properties. To provide a better temperature control, the nephelometer is modified by removing the insulating jacket from the sample chamber and installing two fans with adjustable rotation speed onto the cover. Typically, after 2 h of operation with the lamp turned on, the nephelometer temperature stabilizes at 27.5 ± 0.3 °C. The DMA−DMA system and the CRDS cell are maintained at the same temperature as the nephelometer. The DMA−DMA is enclosed in a temperature-controlled unit. The CRDS cell and all connecting lines are wrapped with Nalgene tubing, and their temperature is kept constant by circulating water. Scattering coefficients measured by the nephelometer and CRDS for nonabsorbing deliquesced ammonium sulfate aerosol (60−85% RH) agree within 5%, confirming that relative humidity inside these instruments is within 1% RH.

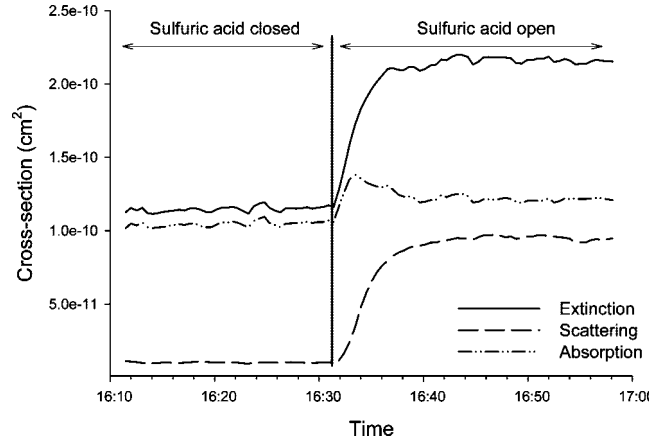

Figure 3. Changes in the extinction, scattering, and absorption cross-sections of soot aerosol (λ = 532 nm) after exposure to the high concentration of sulfuric acid vapor (1.4 × 10^{10} molecule cm^{-3}). The initial (uncoated) particle mobility diameter is 245 nm and relative humidity is 50%. The initial increase in the absorption cross-section after sulfuric acid exposure is an artifact caused by the difference in averaging times of CRDS and the integrating nephelometer.

3. Results and Discussion

3.1. Optical Properties of Fresh and Coated Soot Aggregates. Figure 3 shows the temporal variation of the optical cross-sections for soot particles with initial diameter D_p = 245 nm before and after exposure to the high concentration (1.4 × 10^{10} molecule cm^{-3}) of sulfuric acid vapor. For fresh (unexposed) soot, scattering is weak and the extinction is dominated by absorption, resulting in a single scattering albedo (SSA = C_{sca}/C_{ext}) as low as 0.09. This value is significantly lower than SSA = 0.20 measured for fresh diesel exhaust soot[35] or SSA = 0.24 measured for lightly coated soot in the tropics.[14] Soot formed under the flame conditions used in our study consists of small primary spherules combined into branched aggregates with a low effective density (Table 1). Contrary to the diesel soot and soot observed at low altitudes in the tropical air, these aggregates contain little condensable material volatile at 200 °C and have a fractal dimension D_f = 2.1, characteristic of a relatively open structure.[24] Individual spherules scatter light weakly because their mean diameter (15 nm) is much smaller than the wavelength (λ = 532 nm). Furthermore, since the spherules are loosely connected, scattering by aggregates is weak even though their mobility diameters are comparable with the

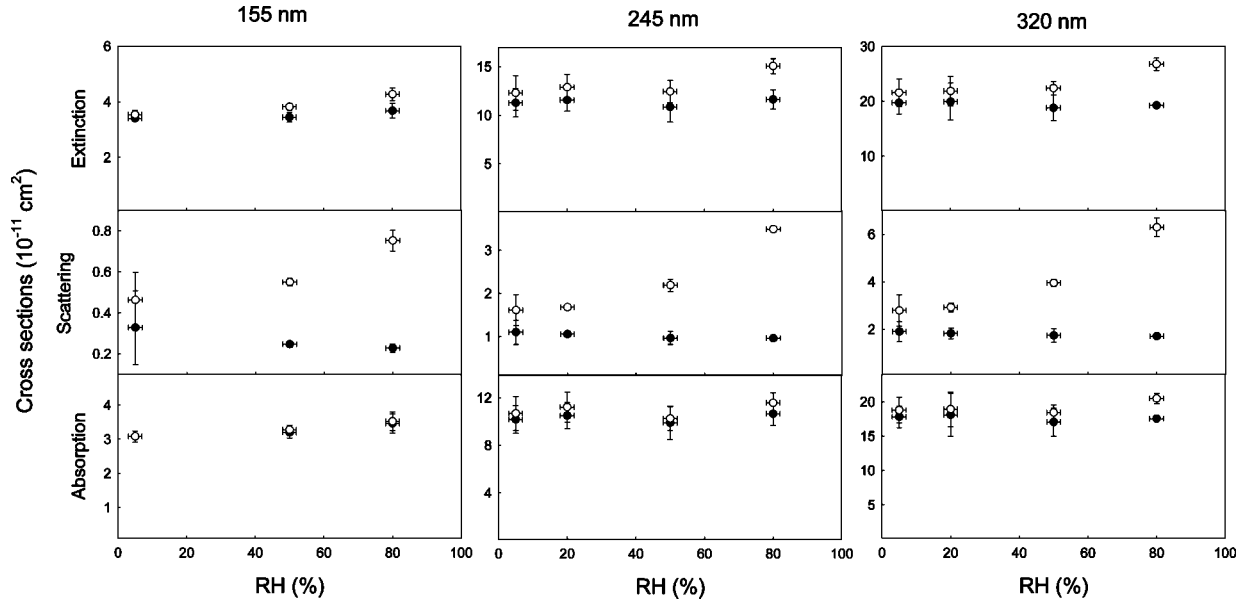

Figure 4. RH dependence of soot extinction, scattering, and absorption cross-sections ($\lambda = 532$ nm) before (solid circles) and after (open circles) exposure of aerosol to the low concentration of sulfuric acid vapor (2.5×10^9 molecules cm^{-3}). The initial (uncoated) particle mobility diameters are 155, 245, and 320 nm.

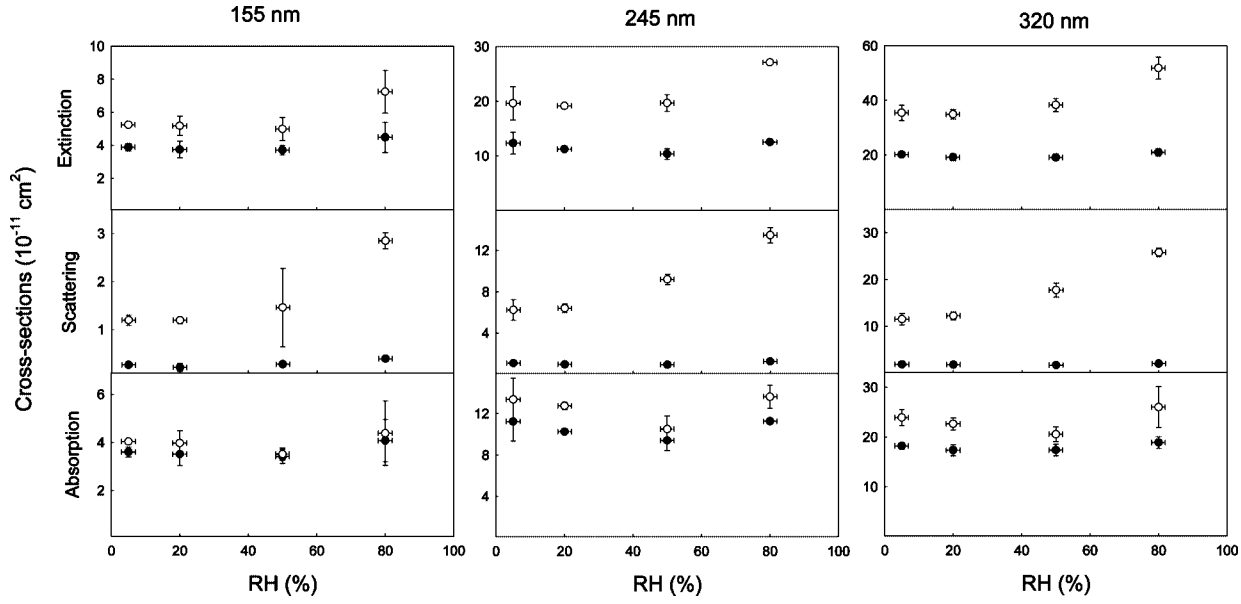

Figure 5. RH dependence of soot extinction, scattering, and absorption cross-sections ($\lambda = 532$ nm) before (solid circles) and after (open circles) exposure of aerosol to the high concentration of sulfuric acid vapor (1.4×10^{10} molecules cm^{-3}). The initial (uncoated) particle mobility diameters are 155, 245, and 320 nm.

light wavelength (the size parameter for aggregates, $x = \pi D_p/\lambda$, is close to unity). When aerosol passes through the H_2SO_4 condensation chamber, soot becomes internally mixed with sulfuric acid and the particle morphology and mixing state are altered,[23,24] leading to a dramatic change in the optical properties. As depicted in Figure 3, at 50% RH light extinction and scattering increase by a factor of 1.9 and 9.7, respectively, yielding a single scattering albedo of 0.47. Also, an increase of about 1.1 is observed for the absorption cross-section at this RH.

The results of optical measurements for soot particles with initial diameters of 155, 245, and 320 nm at the two (high and low) sulfuric acid concentrations and relative humidity from 5 to 80% are presented in Figures 4 and 5. Freshly generated soot is hydrophobic, and its optical properties show only a minor systematic variation with increasing RH, in agreement with our hygroscopicity measurements indicating no change in mobility size and less than $8 \pm 4\%$ increase in mass at 80% RH for fresh soot.[23] For the unprocessed soot aggregates, scattering coefficient is about 1 Mm^{-1}, resulting in the high uncertainty in the measured scattering cross-sections. After exposure of soot to sulfuric acid, a hydrophilic coating is formed on the surface of aggregates and their optical properties become RH-dependent. Scattering and absorption always increase when internal mixing with sulfuric acid occurs, and the observed enhancement is stronger for a higher concentration of sulfuric acid (a larger condensed H_2SO_4 fraction). However, the patterns in the variation in scattering and absorption with increasing RH are somewhat different.

For soot exposed to the low concentration of sulfuric acid (2.5×10^9 molecule cm^{-3}), the H_2SO_4 coating mass fraction is about 0.1, and the scattering cross-section increases exponen-

TABLE 2: Scattering Cross-Sections (λ = 532 nm) of PSL Spheres after Exposure to the High Concentration of Sulfuric Acid Vapor (1.4×10^{10} molecules cm^{-3}) at 20 and 50% RH (initial (uncoated) particle mobility diameter is 152 nm)

			$C_{sca} \times 10^{11}$, cm^2		
RH %	D_p, nm[a]	$n^*(H_2SO_4)$[b]	calculated [c]	measured	error %
5	152	uncoated	3.61	3.91	8.4
20	168	1.489 − 0i	5.99	5.93	−1.0
50	174	1.407 − 0i	6.56	7.05	7.5

[a] Mobility diameters of coated PSL at different RH were calculated using hygroscopic growth factors measured under identical conditions.[23] [b] Calculated using data from ref . [c] Calculated using coated sphere Mie theory, $n^*(PSL) = 1.589 - 0i$.

tially with relative humidity for all particle sizes and at 80% RH becomes 3.3−3.7 times larger than that of fresh soot (Figure 4). The absorption cross-section, on the other hand, shows no visible change for the smallest particles (D_p = 155 nm) and only a very small increase for particles with initial diameters of 245 and 320 nm. Mikhailov et al.[19] reported a similar behavior in scattering and absorption for acetylene soot aggregates that were thinly coated with glutaric acid. For soot particles with the high H_2SO_4 mass fraction (about 0.4), the scattering increases by about 6-fold at 5% RH and as high as 12.6-fold at 80% RH (D_p = 320 nm). The absorption enhancement is size-dependent; absorption increases by 1.1 and 1.4 times at 80% RH for particles with the initial diameters of 155 and 320 nm, respectively. Also, the absorption does not increase monotonously with relative humidity but shows a minimum at about 50% RH (Figure 5). Although both particle mobility size and particle mass change significantly when relative humidity increases from 5 to 80%,[25] absorption cross-sections of H_2SO_4-coated soot particles at low and high RH are comparable. At 80% RH, coated particles show a mobility size growth of about 1.3[23] and fall in region 4 (shells on new particles) according to classification presented by Bond et al.[17] A characteristic feature of this region is that absorption increases immediately after transparent material condenses on carbon soot cores and continues to increase with an additional shell growth. Also, in good agreement with our measurements, the increase in absorption in this region depends on the particle size.[17]

To estimate an overall uncertainty in the derived optical cross-sections of coated soot aerosol at an elevated RH, we measured the scattering of light by PSL spheres with an initial diameter of 152 nm that were exposed to the high concentration of sulfuric acid vapor. The optical properties of both materials, PSL and sulfuric acid, are well-known and hence the measured values can be compared against the theoretical calculations using Mie theory for coated spheres.[36] Table 2 compares the experimental and theoretical scattering cross-sections for coated PSL spheres at 20 and 50% RH. The agreement between the theory and experiment is within 10%, representing uncertainties associated with the relative humidity, particle number density, particle size, and instrument calibration. This error, however, excludes the contribution from multiply charged particle modes because they are absent in the PSL aerosol.

3.2. The Mechanism for Enhancement of Optical Properties. The formation of a transparent shell and compaction of the soot core can both contribute to the increased light scattering and absorption by coated soot particles. To distinguish between these two effects, we measured the change in scattering and absorption by soot subjected to a combination of coating and heating. As shown in Figure 6, heating the fresh (uncoated) soot particles to 200 °C has no effect on scattering but leads to a 1.04−1.14 fold increase in absorption, with smaller values for larger particle sizes. This effect is explainable since absorption by aggregates is increased by about 1.3 times over individual primary spherules,[6] and this factor can be completely or partially

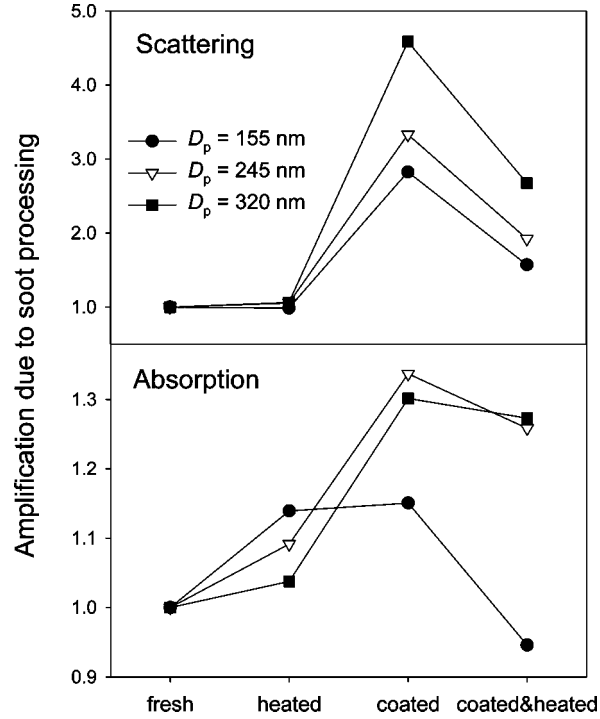

Figure 6. Variations in light scattering and absorption (λ = 532 nm) by soot agglomerates subjected to different types of processing. "Fresh" stands for uncoated soot aerosol, "heated" for soot aerosol that is heated to 200 °C, "coated" for soot aerosol that is exposed to the high concentration of sulfuric acid vapor (1.4×10^{10} molecules cm^{-3}), and "heated&coated" for soot aerosol that is exposed to the high concentration of sulfuric acid vapor and subsequently heated to 200 °C. The initial (uncoated) soot particle mobility diameters are 155, 245, and 320 nm and relative humidity is 5% RH.

lost when particles are thinly coated with nonabsorbing material. Fresh soot aggregates carry a very thin layer of condensed organics so heating the soot removes some or all of the coating, resulting in an increased light absorption. Since the amount of the coated organic material is low for soot used in our experiments, scattering is not affected by heating. This is in agreement with the results of our DMA−APM measurements, indicating that the mass ratio of heated to fresh soot is 0.99 ± 0.04.[24]

Exposure of soot aerosol to sulfuric acid results in a strong enhancement of light scattering. Heating the coated soot particles to remove sulfuric acid reduces the enhancement (Figure 6). However, scattering by coated and heated soot is still significantly higher than scattering by fresh soot. Since the mass of particles that are first coated and then heated is similar to the mass of fresh soot,[24] the increased scattering is caused entirely by irreversible restructuring of the soot cores to a more compact form. Primary spherules in compacted aggregates interact collectively with electromagnetic waves, leading to stronger scattering. Thus, transparent coating affects scattering both

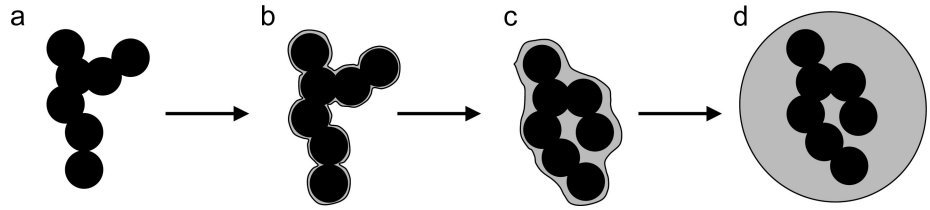

Figure 7. A schematic diagram showing the transformation of soot aggregates with increasing mass fraction of condensed materials.

directly, through increased particle volume, and indirectly, by changing the soot core morphology.

The restructuring is also a major contributor to enhancement of light absorption by soot. Figure 6 shows that for 245 and 320 nm soot particles, enhancement caused by H_2SO_4 coating ($C_{abs}^{coated}/C_{abs}^{fresh} = 1.30-1.34$) is reduced insignificantly by subsequent removal of sulfuric acid through heating ($C_{abs}^{coated\&heated}/C_{abs}^{fresh} = 1.26-1.27$). Soot particles with initial diameter of 155 nm, however, show a smaller increase in absorption after exposure to sulfuric acid, and subsequent heating of these particles reduces absorption to a value slightly below that for fresh soot. The different behavior for large and small aggregates is explained by the effect of restructuring on the interaction between primary spherules and increased effective density of the soot cores caused by processing. When an aggregate collapses to a globule, interaction between neighboring spherules can increase light absorption, and the magnitude of this effect depends on the number and size of primary spherules.[37] However, as the size and density of the collapsed agglomerate increase, the spherules located in the center of the globule become shielded by the outer spherules, leading to decreased absorption cross-section. Coating and heating the 155 nm soot particles increases the density of the cores by more than 3-fold. The density reaches a value of 0.81 g cm^{-3} (ref 24), which is close to the maximum possible density of 1.13 g cm^{-3} for globules that would be formed as a result of complete soot aggregate restructuring. The latter value is calculated as a product of the inherent material density of 1.77 g cm^{-3} for soot[38] and a random close packing factor of 0.637, which is the highest volume fraction of spheres packed to retain a random configuration.[39] The net result of coating and heating in the case of small particles corresponds to nearly complete cancelation between enhancement and shielding caused by restructuring. Larger particles, having lower initial density, experience stronger relative compaction when coated and heated, but the final core densities of 0.66 and 0.48 g cm^{-3} for 245 and 320 nm particles, respectively, are lower than for 155 nm particles. Therefore, the enhancement factor dominates over the shielding, and the absorption cross-section remains above that for fresh soot.

The nonmonotonous behavior of light absorption by coated soot particles with increasing relative humidity (Figure 5) can be explained as competition between water condensation and soot core restructuring, as depicted in Figure 7. When fresh soot aggregates (Figure 7a) are exposed to the low concentration of sulfuric acid, the coating is too thin (Figure 7b) to cause significant absorption enhancement through either lensing or restructuring. As the relative humidity increases, the changing morphology of soot cores and thicker coating due to condensed water both contribute to increased absorption whereas the effect of shielding is still small. Exposure of soot to the high concentration of sulfuric acid vapor produces a thicker coating and leads to large changes in morphology and light absorption even at 5% RH. As the soot cores continue to restructure and become more compact with increasing RH, the enhancement in absorption due to interaction between primary spherules and reduction in absorption caused by shielding act in opposite directions. A minimum in absorption at 50% RH likely corresponds to the nearly complete compaction of H_2SO_4-coated soot aggregates (Figure 7c) observed in TDMA measurements.[23] At this relative humidity, the particle mass increases nearly 3-fold and the effective density, the fractal dimension, and the dynamic shape factor approach values characteristic of spherical particles composed of a compact soot core surrounded by a solution shell.[24] When relative humidity rises above 50%, the increase in absorption is driven almost solely by the growing shell composed of aqueous sulfuric acid (Figure 7d).

Our measurements indicate that restructuring of soot cores represents an important factor in light scattering and absorption by soot aerosol during atmospheric processing. The contribution from restructuring is comparable or even exceeds the effect of lensing by the transparent coating. Depending on the initial size and morphology of fresh soot aggregates (density, fractal dimension, and diameter of primary spherules) and the properties of the coating material, restructuring can act to enhance or reduce the effect of lensing on light absorption. Collapse of aggregates can explain the observed decrease in absorption of soot aerosols with atmospheric lifetime.[5] Several previous studies have addressed the importance of using physically based treatment of carbon soot optics when particles are internally mixed with nonabsorbing material.[6,16,17] However, the complex variation in morphology of soot agglomerates during atmospheric processing has not been taken into account accurately in modeling studies.[40]

3.3. Mass Absorption Cross-Sections of Fresh and Processed Flame Soot. Although black carbon is the major light-absorbing component of atmospheric aerosols, the reported mass absorption cross-sections vary in a wide range due to uncertainties in morphology, density, and the mixing state of soot particles. Our experimental system is designed to measure the optical properties of well-characterized fresh and internally mixed soot aerosol under dry and humid conditions. This approach allows the determination of MAC for size-selected airborne particles with known morphology and mixing state. Table 3 presents mass absorption cross-sections calculated according to eq 4 using fresh soot effective densities given in Table 1. For fresh soot aerosol at 5% RH, the obtained values range from 6.1 to 8.8 m^2 g^{-1}, in good agreement with the value of 7.5 ± 1.2 m^2 g^{-1} ($\lambda = 550$ nm) suggested by Fuller et al.[6] and Bond and Bergstrom[7] on the basis of theoretical calculations and analysis of available measurements. After exposure to sulfuric acid and an elevated relative humidity, MAC increases and becomes as high as 12.6 m^2 g^{-1} in the case of 1.4×10^{10} molecules cm^{-3} concentration of H_2SO_4 vapor and 80% RH.

Mie calculations for single carbon spheres as a function of particle diameter show a maximum in the mass-normalized absorption at about 150 nm (see, for instance, Figure 1 in Bond et al.[17]). Absorption cross-section for particles larger than 150 nm decreases with the inverse of the size because only the surface layer participates in light absorption. For fresh soot in our study, shielding has weaker dependence on the size because

TABLE 3: Mass Absorption Cross-Sections of Soot Aerosol ($\lambda = 532$ nm) before and after Exposure to Low and High Concentration of Sulfuric Acid Vapor

	mass absorption cross-section, $m^2\ g^{-1}$					
	$D_p = 155$ nm		$D_p = 245$ nm		$D_p = 320$ nm	
RH %	fresh	coated	fresh	coated	fresh	coated
$H_2SO_4 = 2.5 \times 10^9$ Molecules cm^{-3}						
5	6.1 ± 0.3	6.1 ± 0.1	7.9 ± 0.9	8.3 ± 1.1	8.6 ± 0.8	9.1 ± 0.9
20	7.9 ± 0.4	8.2 ± 0.4	8.1 ± 0.9	8.7 ± 1.0	8.8 ± 1.5	9.2 ± 1.2
50	6.4 ± 0.3	6.5 ± 0.3	7.7 ± 1.1	7.9 ± 0.8	8.3 ± 1.0	8.9 ± 0.5
80	6.9 ± 0.6	7.0 ± 0.5	8.2 ± 0.8	9.0 ± 0.7	8.5 ± 0.1	9.9 ± 0.4
$H_2SO_4 = 1.4 \times 10^{10}$ Molecules cm^{-3}						
5	7.2 ± 0.4	8.0 ± 0.1	8.7 ± 1.5	10.3 ± 1.6	8.8 ± 0.3	11.6 ± 0.8
20	7.0 ± 0.9	7.9 ± 1.0	7.9 ± 0.2	9.9 ± 0.3	8.4 ± 0.5	11.0 ± 0.6
50	6.8 ± 0.6	7.0 ± 0.5	7.3 ± 0.8	8.1 ± 1.0	8.4 ± 0.6	10.0 ± 0.7
80	8.1 ± 1.7	8.7 ± 2.7	8.7 ± 0.1	10.6 ± 0.9	9.2 ± 0.6	12.6 ± 2.0

the aggregates are composed of loosely connected small primary spherules, and hence MAC increases with particle mobility size.

Table 3 shows a small systematic difference between absorption cross-sections for fresh soot, ranging from 2% (320 nm particles) to 15% (155 nm particles). A range of factors may contribute to the observed discrepancy, including variations in soot generation, dilution, sizing, optical instrument calibration, and particle counting. Since the optical measurements for PSL spheres performed along with soot measurements show a good agreement, the source of discrepancy likely relates to soot generation in the flame. One possibility is the presence of a light-absorbing gaseous species produced by the flame, such as NO_2, whose concentration can change with the flame equivalence ratio and sample dilution. However, a separate test performed with DMA1 and DMA2 voltages set to transmit no soot particles shows no change in the extinction or scattering backgrounds when clean nitrogen is substituted for the flame-generated soot aerosol. This leaves the variation in the soot particle morphology and mixing state as the only source for the observed discrepancy. Although a constant flame equivalence ratio and particle size distributions are maintained throughout all optical measurements, the optical properties of soot aerosol are very sensitive to the density and mixing state, and hence a small variation in the flame equivalence ratio or sample dilution can lead to the observed systematic difference in MAC. Schnaiter et al.[41] reported a drastic dependence of absorption cross-section of soot aerosol on the flame equivalence ratio and particle size. Also, smaller sizes have been found to be more strongly affected because of the appearance of smaller organic particles at higher flame equivalence ratios, leading to significantly lower absorption cross-sections.

3.4. Atmospheric Implications. Mass absorption cross-sections for fresh soot aggregates are size dependent, increasing from 6.7 ± 0.7 to 8.7 ± 0.8 $m^2\ g^{-1}$ for particles with mobility diameters from 155 to 320 nm (average MAC values between two series of measurements). During atmospheric aging in the presence of sulfuric acid with the concentrations of 10^5-10^7 molecule cm^{-3}, it will take freshly emitted soot from 5 h to 3 d to become internally mixed with 10−40% sulfate coating by mass.[24] When soot acquires such a mass fraction of sulfate coating, absorption increases to $9-12$ $m^2\ g^{-1}$, in agreement with ambient values measured in polluted regions.[5] It should be pointed out that condensation of organic matter on soot particles may also occur in the atmosphere, changing particle morphology and optical properties.[18] However, it is likely that sulfuric acid will have an effect much larger than that of organics because condensation of H_2SO_4 largely determines the aerosol hygroscopicity and hence the ability of particles to absorb water and change particle morphology.

A significant part of enhancement of light absorption and scattering by soot during atmospheric processing arises from the changes in the particle morphology. Increased absorption is accompanied by a large increase in scattering, which is reflected in a single scattering albedo rising from 0.1 for fresh soot to 0.5 for processed soot. Hence, formation of a transparent coating may not necessarily result in an increased positive forcing by coated soot aerosol. A rigorous estimate of radiative forcing requires explicit modeling of the aerosol dynamics. Also, since the change in morphology of soot cores is irreversible, even slightly hygroscopic soot particles (a small fraction of water soluble material) that are subjected to cloud processing will exhibit altered optical properties after evaporation of cloud droplets.

Our results imply that in polluted air the optical properties of soot particles are considerably enhanced because of condensation of sulfuric acid and correlate strongly with RH. The enhanced absorption due to internal mixing of soot with sulfate will reduce photolysis rates in the planetary boundary layer when air pollution is highest, leading to lower ground level ozone concentration.[3] Also, enhanced light absorption and scattering stabilize the atmosphere because of cooling at the earth surface and warming aloft. This will have an important feedback on air quality, since a stable atmosphere retards vertical transport.[42] Less surface heating and atmospheric stabilization will also impact the cloud dynamics. Reduction in vertical sensible and latent heat exchanges and restricted convective development will decrease the formation of clouds, whereas warming in the atmosphere can evaporate the existing cloud droplets by lowering the relative humidity.[4,43]

4. Conclusions

We have investigated the optical properties of carbon soot during simulated atmospheric processing. Internally mixed soot aerosol with a known morphology and mixing state is produced by exposure of flame-generated, size-selected soot particles to gaseous sulfuric acid (10^9-10^{10} molecule cm^{-3}). Coated airborne soot particles are subjected to elevated humidity environment and the light extinction, scattering, and absorption cross-sections at 532 nm are determined using a combination of a cavity ring-down spectrometer and an integrating nephelometer.

The optical properties of fresh (uncoated) soot are practically independent of relative humidity (RH). Exposure of soot to sulfuric acid causes particle growth by water condensation, leading to significant enhancement in light absorption and scattering even at low RH. Scattering of light by coated soot particles increases exponentially with relative humidity. Absorption, on the other hand, displays a minimum at a relative

humidity corresponding to about 2.5-fold particle mass increase from condensed sulfuric acid and water. For soot particles with an initial mobility diameter of 320 nm and a 40% H_2SO_4 coating mass fraction, absorption and scattering are enhanced 1.4- and 13-fold at 80% RH, resulting in a single scattering albedo increase from 0.1 to 0.5.

The irreversible restructuring of soot aggregates caused by condensation of sulfuric acid and water can alter both scattering and absorption. Depending on the initial size and density of soot aggregates, restructuring acts to increase or decrease the absorption enhancement. However, the effect of encapsulation always dominates over restructuring, resulting in an increased absorption cross-section for internally mixed soot.

Mass absorption cross-sections for fresh soot aggregates are size dependent, increasing from 6.7 ± 0.7 m^2 g^{-1} for 155 nm particles to 8.7 ± 0.8 m^2 g^{-1} for 320 nm particles. When soot particles acquire about 10−40% sulfate coating by mass, absorption increases to 9−12 m^2 g^{-1} in agreement with ambient values measured in polluted regions. Our results imply that optical properties of soot are significantly altered within its atmospheric lifetime, leading to greater impact on visibility, local air quality, and radiative climate forcing.

Acknowledgment. This work was supported by the US Department of Energy National Institute for Climate Change Research (DOE - NICCR) and Robert A. Welch Foundation. R.Z. acknowledges additional support from National Natural Science Foundation of China Grant (40728006).

References and Notes

(1) IPCC (Intergovernmental Panel on Climate Change). Report. Solomon, S., et al., Eds.; Cambridge Univ. Press, Cambridge, UK, 2007. http://www.ipcc.ch/ipccreports/ar4-wg1.htm.
(2) Ramanathan, V.; Carmichael, G. *Nature Geosci.* **2008**, *1*, 221.
(3) Li, G. H.; Zhang, R. Y.; Fan, J. W.; Tie, X. X. *J. Geophys. Res.* **2005**, *110*, D23206.
(4) Fan, J. W.; Zhang, R. Y.; Tao, W. K.; Mohr, K. I. *J. Geophys. Res.* **2008**, *113*, D08209.
(5) Liousse, C.; Cachier, H.; Jennings, S. G. *Atmos. Environ.* **1993**, *27*, 1203.
(6) Fuller, K. A.; Malm, W. C.; Kreidenweis, S. M. *J. Geophys. Res.* **1999**, *104*, 15941.
(7) Bond, T. C.; Bergstrom, R. W. *Aerosol Sci. Technol.* **2006**, *40*, 27.
(8) Zhang, D.; Zhang, R. *Environ. Sci. Technol.* **2005**, *39*, 5722.
(9) Levitt, N. P.; Zhang, R. Y.; Xue, H. X.; Chen, J. M. *J. Phys. Chem. A* **2007**, *111*, 4804.
(10) Kotzick, R.; Niessner, R. *Atmos. Environ.* **1999**, *33*, 2669.
(11) Zuberi, B.; Johnson, K. S.; Aleks, G. K.; Molina, L. T.; Laskin, A. *Geophys. Res. Lett.* **2005**, *32*, L01807.
(12) Olfert, J. S.; Symonds, J. P. R.; Collings, N. *J. Aerosol Sci* **2007**, *38*, 69.
(13) Shiraiwa, M.; Kondo, Y.; Moteki, N.; Takegawa, N.; Miyazaki, Y.; Blake, D. R. *Geophys. Res. Lett.* **2007**, *34*, L16803.
(14) Schwarz, J. P.; Spackman, J. R.; Fahey, D. W.; Gao, R. S.; Lohmann, U.; Stier, P.; Watts, L. A.; Thomson, D. S.; Lack, D. A.; Pfister, L.; Mahoney, M. J.; Baumgardner, D.; Wilson, J. C.; Reeves, J. M. *J. Geophys. Res.* **2008**, *113*, D03203.
(15) Jacobson, M. Z. *Geophys. Res. Lett.* **2000**, *27*, 217.
(16) Jacobson, M. Z. *Nature* **2001**, *409*, 695.
(17) Bond, T. C.; Habib, G.; Bergstrom, R. W. *J. Geophys. Res.* **2006**, *111*, D20211.
(18) Schnaiter, M.; Linke, C.; Mohler, O.; Naumann, K. H.; Saathoff, H.; Wagner, R.; Schurath, U.; Wehner, B. *J. Geophys. Res.* **2005**, *110*, D19204.
(19) Mikhailov, E. F.; Vlasenko, S. S.; Podgorny, I. A.; Ramanathan, V.; Corrigan, C. E. *J. Geophys. Res.* **2006**, *111*, D07209.
(20) Gangl, M.; Kocifaj, M.; Videen, G.; Horvath, H. *Atmos. Environ.* **2008**, *42*, 2571.
(21) Zhang, R.; Wooldridge, P. J.; Abbatt, J. P. D.; Molina, M. J. *J. Phys. Chem.* **1993**, *97*, 7351.
(22) Middlebrook, A. M.; Iraci, L. T.; McNeill, L. S.; Koehler, B. G.; Wilson, M. A.; Saastad, O. W.; Tolbert, M. A.; Hanson, D. R. *J. Geophys. Res.* **1993**, *98*, 20473.
(23) Khalizov, A. F.; Zhang, R.; Zhang, D.; Xue, H.; Pagels, J.; McMurry, P. H. J. Geophys. Res. 2008, in press.
(24) Zhang, R.; Khalizov, A. F.; Pagels, J.; Zhang, D.; Xue, H.; McMurry, P. H. *Proc. Natl. Acad. Sci. U.S.A.* **2008**, *105*, 10291.
(25) Suh, I.; Zhang, R.; Molina, L. T.; Molina, M. J. *J. Am. Chem. Soc.* **2003**, *125*, 12655.
(26) Santoro, R. J.; Semerjian, H. G.; Dobbins, R. A. *Combust. Flame* **1983**, *51*, 203.
(27) Kasper, M.; Siegmann, K.; Sattler, K. *J. Aerosol Sci* **1997**, *28*, 1569.
(28) Kirchstetter, T. W.; Novakov, T. *Atmos. Environ.* **2007**, *41*, 1874.
(29) Fortner, E. C.; Zhao, J.; Zhang, R. Y. *Anal. Chem.* **2004**, *76*, 5436.
(30) Zhang, R. Y.; Suh, I.; Zhao, J.; Zhang, D.; Fortner, E. C.; Tie, X. X.; Molina, L. T.; Molina, M. J. *Science* **2004**, *304*, 1487.
(31) Zhao, J.; Zhang, R. Y.; Fortner, E. C.; North, S. W. *J. Am. Chem. Soc.* **2004**, *126*, 2686.
(32) Orsini, D. A.; Wiedensohler, A.; Stratmann, F.; Covert, D. S. *J. Atmos. Ocean. Technol.* **1999**, *16*, 760.
(33) Smith, J. D.; Atkinson, D. B. *Analyst* **2001**, *126*, 1216.
(34) Anderson, T. L.; Ogren, J. A. *Aerosol Sci. Technol.* **1998**, *29*, 57.
(35) Schnaiter, M.; Horvath, H.; Mohler, O.; Naumann, K. H.; Saathoff, H.; Schock, O. W. *J. Aerosol Sci.* **2003**, *34*, 1421.
(36) Bohren, C. F.; Huffman, D. R. *Absorption and scattering of light by small particles*; Wiley: New York, 1983.
(37) Iskander, M. F.; Chen, H. Y.; Penner, J. E. *Atmos. Environ.* **1991**, *25*, 2563.
(38) Park, K.; Kittelson, D. B.; Zachariah, M. R.; McMurry, P. H. *J. Nanopart. Res.* **2004**, *6*, 267.
(39) Feder, J. *Fractals*; Plenum Press: New York, 1988.
(40) Liu, Y. H.; Daum, P. H *J. Aerosol Sci.* **2008**, *39*, 974.
(41) Schnaiter, M.; Gimmler, M.; Llamas, I.; Linke, C.; Jager, C.; Mutschke, H. *Atmos. Chem. Phys.* **2006**, *6*, 2981.
(42) Zhang, R.; Lei, W. F.; Tie, X. X.; Hess, P. *Proc. Natl. Acad. Sci. U.S.A.* **2004**, *101*, 6346.
(43) Zhang, R.; Li, G.; Fan, J.; Wu, D. L.; Molina, M. J. *Proc. Natl. Acad. Sci. U.S.A.* **2007**, *104*, 5295–5299.
(44) Tang, I. N. *J. Geophys. Res.* **1996**, *101*, 19245.

JP807531N